PHOTONICS Research

Four-wave mixing in graphdiyne-microfiber based on synchronized dual-wavelength pulses

XINXIN JIN,[1,2,†] WENLI BAO,[3,†] HAN ZHANG,[3] ZHENG ZHENG,[1] AND MENG ZHANG[1,*]

[1]School of Electronic and Information Engineering, Beihang University, Beijing 100191, China
[2]College of Electrical and Electronic Engineering, Wenzhou University, Wenzhou 325035, China
[3]International Collaborative Laboratory of 2D Materials for Optoelectronics Science and Technology of Ministry of Education, College of Optoelectronic Engineering, Shenzhen University, Shenzhen 518060, China
*Corresponding author: mengzhang10@buaa.edu.cn

Received 1 October 2021; revised 25 November 2021; accepted 15 December 2021; posted 16 December 2021 (Doc. ID 444938); published 1 February 2022

We demonstrate four-wave mixing (FWM) in the graphdiyne (GDY) microfiber based on the synchronized dual-wavelength pump pulses that are transformed from a mode-locked fiber laser. Benefiting from the large nonlinear refractive index of GDY and the synchronized pump pulses, a maximum conversion efficiency of −39.05 dB can be achieved in GDY with only an average pump power of 6.9 mW, greatly alleviating the possible damage compared to previous investigations employing the continuous-wave pump. In addition, our proposal can be applied to measure the effective nonlinear coefficient γ of the GDY-microfiber, which could be extended as a practical measurement tool for γ of nanomaterials-based devices.

https://doi.org/10.1364/PRJ.444938

1. INTRODUCTION

Graphdiyne (GDY), a novel 2D carbon allotrope formed by the hybridization of sp and sp^2 carbons, features a variety of outstanding characteristics such as high electron and hole mobility, direct natural band gap, and superior thermal stability [1], which benefit its application in numerous fields such as batteries [2], biomedicine [3], catalysis [4], and photodetectors [5,6]. Compared to zero band gap graphene, GDY has a natural band gap energy calculated to be between 0.46 and 1.22 eV [7–9], endowing itself as an excellent semiconductor material for electronic devices. Recently, GDY has attracted considerable attention in photonic and optoelectronic applications with the discovery of their broad band working wavelength and high optical nonlinear susceptibility [10–12]. The third-order susceptibility is a complex quantity, where the real part is responsible for the Kerr effect that leads to a number of nonlinear phenomena such as self-phase modulation (SPM), cross-phase modulation (XPM), and four-wave mixing (FWM); the imaginary part is responsible for nonlinear absorption. The saturable absorption effect of the 2D material family has been extensively investigated for mode-locking pulsation since 2009 [13–15], and great progress has been made in the field of high-order harmonic ultrashort pulse generation [16–20]. The first demonstration, to the best of our knowledge, of GDY used as a saturable absorber for pulse generation in femtosecond level was reported by Zhao *et al.*, which opens up a path for its application in ultrafast photonics and optoelectronics [21]. Recently, the growing prospect of the exploitation of nonlinear Kerr effects in 2D materials for all-optical signal processing has triggered intense research interests in the application of the real part of third-order susceptibility. Among these nonlinear phenomena, FWM is particularly valued, as it offers application scopes in wavelength conversion, frequency comb generation, supercontinuum generation, and optical parametric amplification [22]. The nonlinear refractive index n_2 of GDY ($\sim 10^{-9}$ m^2/W) is large among various 2D materials such as graphene ($\sim 10^{-11}$ m^2/W), antimonene ($\sim 10^{-19}$ m^2/W), and MoS_2 ($\sim 10^{-10}$ m^2/W) [10,23–25]. This offers opportunities towards the development of GDY-enabled FWM devices with compact size. The reported length of nanomaterial-based FWM devices that employ a lateral interaction structure (e.g., microfiber or side-polished fiber) varies from hundreds of micrometers (μm) to a few centimeters (cm) [24,26–29]. In addition, the GDY is constituted by the sp and sp^2 hybridized alkyne bonds and benzene rings [30], where the high π conjugation endows GDY with superior stability. Thus, GDY can effectively prevent its photo-oxidation and photodegradation under strong light exposure, which is pursued in fabricating stable optical devices. For comparison, although the n_2 of black phosphorus (BP) is at the same order as that of GDY [31], the application of BP generally needs additional steps such as encapsulation and surface coordination to guarantee its stability due to the intrinsic instability of phosphorene under ambient conditions [32–35], which increases the fabrication complexity of the device.

The typical all-fiber scheme for nanomaterial-based FWM employs two continuous-wave (CW) lasers as the pump, and the total pump power ranges from a few hundred milliwatts (mW) to as high as several watts (W) [36]. The heat cumulated from such high CW power can induce damage to the nanomaterials and their substrate, however, the conversion efficiency is still limited. An effective way to reduce the pump power and improve the conversion efficiency would suggest use of a pulse-pulse pump, replacing the CW sources altogether. However, compared to the CW-CW source, where interaction between the two beams is always satisfied, the pulse-pulse pump strictly requires that the two pulse trains arrive at the nonlinear device simultaneously. In other words, the two pulse trains should be synchronized in both time (i.e., possessing the same repetition frequency) and space (i.e., propagating without time delay). So far, most of the schemes for synchronous ultrashort pulses generation are based on the synchronization of two oscillators [37–39]. The mismatch length of these schemes is sensitive to the environmental perturbations. In addition, the pulses from these schemes are only synchronized in time, while the synchronization in space cannot be obtained due to the chromatic dispersion in the fiber. A simple and low-cost solution to produce a suitable pump source remains challenging.

Here, we propose an all-fiber FWM scheme using a dual-wavelength pulse-pump that is synchronized in both time and space. The dual-wavelength pulses are filtered from an erbium-doped (Er-doped) mode-locked fiber laser (MLFL) and then synchronized in space by an optical delay line. Thanks to the high peak power of the pulse-pump, FWM conversion efficiency of −39.05 dB in GDY can be achieved under a low average pump power of 6.9 mW, overcoming the drawback of the CW-pump scheme. We also find an application for our FWM scheme in calculating the effective nonlinear coefficient γ of the integrated GDY microfiber.

2. CHARACTERIZATION OF GDY

The GDY film on copper foil is prepared via Glayser–Hay coupling according to Li's methods [1].

The morphology characterizations of GDY are shown in Fig. 1. Figure 1(a) exhibits the SEM image of GDY. The high-resolution transmission electron microscopy (HR-TEM) image of GDY is shown in Fig. 1(b), where the inset shows the corresponding selected area electron diffraction (SAED) pattern, which represents orderly layered 2D material. Figure 1(c) manifests the Raman spectra of the as-prepared GDY film, as the 1360 cm^{-1} and 1575 cm^{-1} peaks referred to the D and G bands, which were related to the stretching vibration of aromatic rings. The X-ray photoelectron spectroscopy (XPS) profiles of the narrow scan for element C included four subpeaks of C 1s at 284.4, 284.9, 286.2, and 288.5 eV, representing the orbitals in C-C (sp^2), C-C (sp), C-O, and C = O bonds, respectively, in Fig. 1(d).

3. EXPERIMENTAL SETUP

The proposed all-fiber FWM scheme is shown in Fig. 2. The experimental setup consists of two main parts. The first part is an Er-doped fiber (EDF) laser mode-locked by nonlinear polarization evolution (NPE). A 1.03 m long Liekki Er80-8/125 EDF is used as the gain medium that is pumped by a 980 nm laser diode. The ring cavity also consists of a

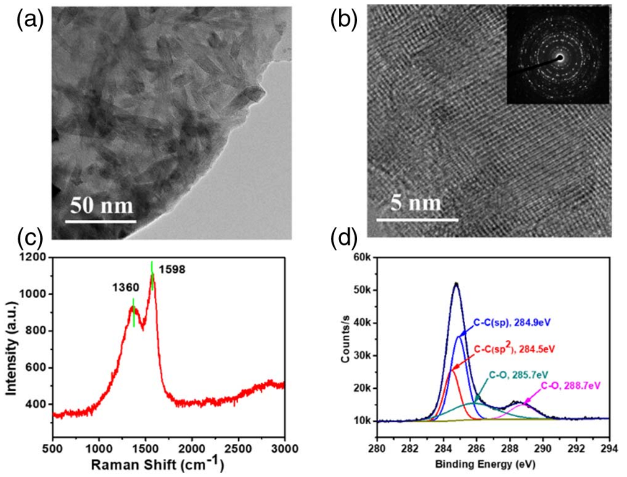

Fig. 1. Morphology characterizations of GDY. (a) SEM image of GDY; scale bar: 50 nm. (b) HR-TEM image of GDY; scale bar: 5 nm. Inset shows the corresponding SAED pattern. (c) Raman spectrum of the as-prepared GDY film. (d) XPS spectra of GDY film: narrow scan for element C.

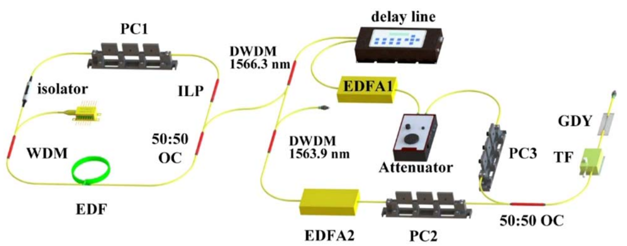

Fig. 2. Schematic of the FWM in GDY-microfiber based on synchronized dual-wavelength pulses. WDM, wavelength division multiplexer; EDF, Er-doped fiber; OC, optical coupler; ILP, inline polarizer; PC, polarization controller; DWDM, dense wavelength division multiplexer; EDFA, Er-doped fiber amplifier; TF, tunable filter.

three-paddle polarization controller (PC) that adjusts the polarization of the pulse in the cavity, an inline polarizer (ILP) that allows only one polarization state to pass through, an isolator that ensures unidirectional circulating of the light, and an optical coupler (OC) that delivers 50% power to the second part. The MLFL has a total length of 5.68 m and a net cavity dispersion of −0.115 ps^2. Figure 3(a) shows the mode-locked spectrum at 1565.3 nm with an output power of 6.5 mW from the MLFL.

The second part of the scheme transforms the pulses from the first part to be synchronized dual-wavelength pulses. The pulses from the MLFL are firstly filtered by a dense wavelength division multiplexer (DWDM) with a pass channel at 1566.3 nm and channel spacing of 100 GHz. The signals from the reflection channel of the first DWDM are then delivered to the second DWDM with pass channel at 1563.9 nm and channel spacing of 100 GHz. As the pulse trains selected by the two DWDMs are filtered from the same mode-locked laser, they possess the same repetition frequency (i.e., synchronized in

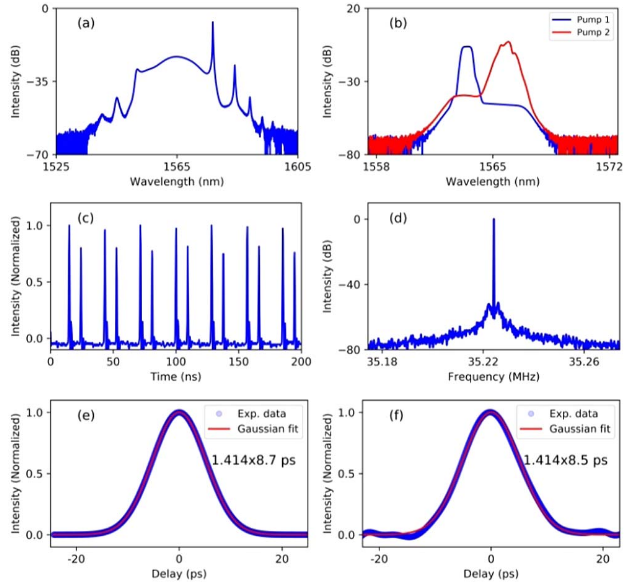

Fig. 3. Characteristics of the pump. (a) Mode-locked spectrum from the MLFL. (b) Spectrum of the dual-wavelength pump after the tunable filter. (c) Oscilloscope trace of the two pulse trains. (d) RF spectrum on a span of 100 kHz. Autocorrelation trace of (e) pump1 and (f) pump2.

time). However, the same repetition frequency cannot guarantee space synchronization due to the different fiber lengths of the two paths. An optical delay line with 330 ps tuning range is thus inserted after the first DWDM to compensate the length mismatch. The two pulse-trains are then amplified by the two EDF amplifiers (EDFAs), respectively. An attenuator is inserted to adjust the amplified power from EDFA1. PC2 and PC3 are used to adjust the phase matching between the two pulse trains when they are combined by the 3 dB OC.

The tunable band-pass filter with a bandwidth of 3.2 nm suppresses the FWM signal brought by the fiber pigtail of the OC and the massive amplified spontaneous emission (ASE) brought by the EDFAs. The optical spectrum of the dual-wavelength pulses after the tunable filter shows central wavelengths of 1563.9 nm (termed as pump1) and 1566.27 nm (termed as pump2), respectively [Fig. 3(b)], where full width at half-maximum of the bandwidth is 0.64 nm and 0.66 nm, respectively. The oscilloscope trace and radio frequency (RF) spectrum are shown in Figs. 3(c) and 3(d), respectively. The two pulse trains on the oscilloscope have a fixed distance [Fig. 3(c)], and the RF spectrum shows a single fundamental frequency of ~35.22 MHz with a signal to noise ratio (SNR) >50 dB [Fig. 3(d)]. Both the oscilloscope trace and RF spectrum confirm that the two pulse trains are synchronized with the same repetition frequency. We note that Fig. 3(c) is recorded by removing the 2.76 m attenuator to distinguish the two pulse trains on the oscilloscope. The pulse duration, measured by an autocorrelator, is 8.7 ps for pump1 and 8.5 ps for pump2 [Figs. 3(e) and 3(f)]. The time bandwidth products of the two pulses are calculated to be 0.7, which indicates that the pulses are chirped. With the measured average power of 2.26 mW and 4.67 mW, the peak power of the two pulses is calculated to be 7.37 W and 15.6 W, respectively. The GDY deposited on the

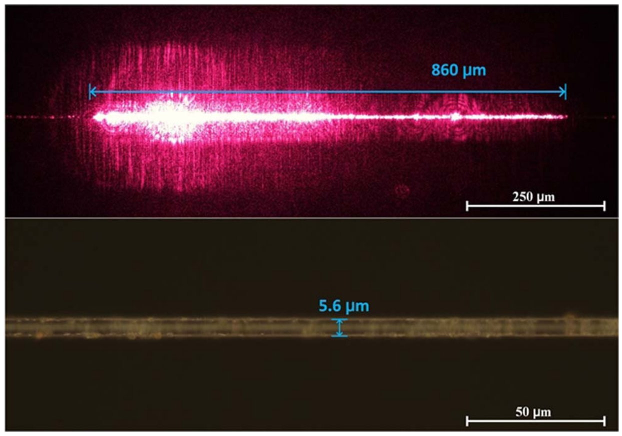

Fig. 4. Optical microscope image of the GDY-microfiber device. The upward image shows the GDY-microfiber with 650 nm laser injected, where the deposition length of 860 μm could be inferred from the region of the scattered light. The downward image shows the microfiber deposited with GDY.

microfiber (GDY-microfiber) is employed as the nonlinear device here for FWM generation. The microfiber is fabricated by stretching the standard single-mode fiber (SMF-28e) under an oxy-hydrogen flame. The GDY is deposited on the tapered fiber by an optical deposition method. The loss is 0.42 dB for the bare microfiber and increases to 1.59 dB after optical deposition with GDY. Figure 4 shows the optical microscopic image of the fabricated sample with a deposition length of 860 μm and a taper waist diameter of 5.6 μm.

4. FWM RESULTS

With the pump scheme described in Section 3, we firstly perform the experiment with the bare microfiber without GDY. When the delay line is properly tuned so that the two pump-pulses are exactly synchronized in the space, signals with different wavelengths arise in the spectrum. The new frequency signals could be further optimized to the maximum by properly setting PC2 and PC3 for phase matching [Fig. 5(a)]. According to the energy conservation of the FWM theory [22], we confirm that the generated signals at the short wavelength of 1561.5 nm and the long wavelength of 1568.6 nm are the first-order anti-Stokes bands and the first-order Stokes bands, respectively. In this case, the FWM signal is completely contributed by fibers, and the conversion efficiency is −34.99 dB (the 0.42 dB loss of the microfiber is included).

We then perform the experiment again with the GDY-microfiber while the other components in the experiment maintain unchanged. The pump passing through the GDY-microfiber is 1.17 dB lower due to the absorption of the GDY, while the intensity of first-order anti-Stokes bands and Stokes bands is improved by 0.634 dB [Fig. 5(a)]. The FWM conversion efficiency is −34.36 dB (the 0.42 dB loss of the microfiber and the 1.17 dB absorption of the GDY are included). We note that the intensity of the FWM signals is actually improved by 1.804 dB (1.17 + 0.634 dB) when considering that the GDY can also cause 1.17 dB loss to the FWM signal contributed by fibers. Thus, we deduce that GDY contributes

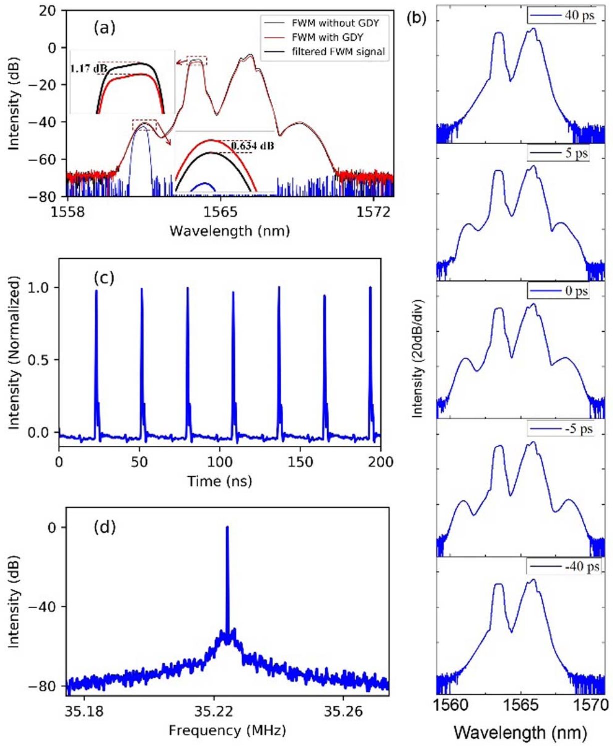

Fig. 5. Results of the FWM experiments. (a) FWM spectra without GDY (black line), with GDY (red line), and of the filtered first-order anti-Stokes signal (blue line). (b) FWM spectrum versus different delay between the two pump-pulses. (c) The oscilloscope trace and (d) RF spectrum of the filtered first-order anti-Stokes signal.

34% to the whole FWM signal, and the true conversion efficiency of GDY alone is −39.05 dB. The spectral variations versus time delay are recorded in Fig. 5(b), where we define the time delay that results in maximum signals as "0 ps." The new frequency signals would be faded out when the time delay is tuned away from 0 ps, indicating that the signals are indeed generated by FWM. We note that the first-order Stokes and anti-Stokes bands do not center at the exact same wavelength, as the delay is changed from −5 ps to 0 ps and to 5 ps. We attribute this to the chirp of the pump pulses. When the delay is <0 ps, the leading edge of pump1 interacts with the trailing edge of pump2; and the situation is opposite when the delay is >0 ps. As pulses are chirped, frequencies are different at the leading edge and trailing edge, leading to the first-order Stokes and anti-Stokes bands centered at the different wavelengths. The first-order anti-Stokes signal is then filtered out by a DWDM with center wavelength of 1561.4 nm when delay =0 ps [Fig. 5(a)]. The oscilloscope trace of the filtered signal is a set of pulse trains, which would be vanished by changing the time delay, indicating that the pulse signal indeed belongs to the first-order anti-Stokes band other than incomplete isolation from the pump [Fig. 5(c)]. The RF of the filtered signal centered at 35.22 MHz has an SNR > 50 dB [Fig. 5(d)].

5. DISCUSSION

According to the FWM theory, the frequency of the newly generated signal should match $2\omega_i - \omega_j$ and $2\omega_j - \omega_i$, respectively, where ω_i and ω_j are the frequency of the pump. Thus, the wavelength of the newly generated signal should be $\lambda_i\lambda_j/(2\lambda_j - \lambda_i)$ and $\lambda_i\lambda_j/(2\lambda_i - \lambda_j)$, respectively, where λ_i and λ_j are the wavelength of the pump. By substituting the pump wavelength of 1563.9 nm and 1566.27 nm into the formula, the newly generated signal should be at 1561.5 nm and 1568.6 nm, respectively, which are consistent with our experimental results. The FWM conversion efficiency R is determined by the following equation [40]:

$$R = \eta P_1 P_2 (\gamma L)^2 \exp(-\alpha L), \tag{1}$$

where P_1 and P_2 are the power of the pump, L is the light propagation length, α is the absorption, γ is the effective nonlinear coefficient, and η is the transition effectivity given as

$$\eta = \frac{1}{1 + (\Delta k/\alpha)^2} \left\{ 1 + \frac{4 \exp(-\alpha L)\sin^2(\Delta k L/2)}{[1 - \exp(-\alpha L)]^2} \right\}, \tag{2}$$

where Δk is the phase-matching factor expressed as

$$\Delta k = \frac{\lambda_k^2}{2\pi c}(\omega_i - \omega_j)^2 \left[D_c + \frac{\lambda_k^2}{2\pi c}(|\omega_i - \omega_j|)\frac{\mathrm{d}D_c}{\mathrm{d}\lambda} \right], \tag{3}$$

where D_c is the chromatic dispersion, $\mathrm{d}D_c/\mathrm{d}\lambda$ is the dispersion slope, and λ_k ($k = i, j$) is the wavelength corresponding to the wave at frequency. The chromatic dispersions of the bare microfiber and GDY-microfiber are calculated by the finite-difference eigenmode (FDE) solver, where the boundary conditions are set as a perfectly matched layer. The chromatic dispersion and the dispersion slope of the microfiber are calculated as 10.5 ps/(nm · km) and 0.02 ps/(nm^2 · km), respectively. The chromatic dispersion and the dispersion slope of the GDY-microfiber are calculated as −85 ps/(nm · km) and −0.4 ps/(nm^2 · km), respectively. The absorptions of the microfiber and GDY-microfiber are 112.5 m^{-1} and 431.5 m^{-1}, respectively. Substituting the above values into the Eq. (3), the phase-matching factors of the microfiber and GDY-microfiber are calculated to be 0.052 m^{-1} and −0.4 m^{-1}, respectively. However, the change in phase-matching factor has little effect on the transition effectivity η. The η of the microfiber and GDY-microfiber are both calculated to be ≈1 with a difference on the order of 10^{-8}. This result can also be estimated as follows: the term $(\Delta k/\alpha)^2$ in Eq. (2) is on the order of 10^{-7}, and the second term in the bracket of the right side of the Eq. (2), whose value is limited by the term $\sin^2(\Delta k L/2)$, is also on the order of 10^{-7}. Thus, the η could be considered as one despite that the device is coated with GDY or not. The gain in FWM conversion efficiency of the GDY-microfiber compared to the bare microfiber is mainly due to the improvement of nonlinear coefficient γ other than the change in phase matching. This conclusion is consistent with previous reports [36,41].

γ of the device is closely relevant to n_2 of the materials and the structure of the device. Table 1 shows typical results of FWM based on 2D materials, where the pump power, n_2 of the materials, and the geometric parameters of these devices are also presented. Although the n_2 of BP and GDY are at the same order, the maximum conversion efficiency of −39.05 dB obtained in this work is still improved by two orders of magnitude with only 6.93 mW average pump power. Our synchronized dual-wavelength pulse scheme is thus of great advantage in improving FWM conversion efficiency with a low

Table 1. Four-Wave Mixing Phenomenon Experimentally Demonstrated in 2D Materials

Sample	n_2 (m^2/W)	Structure	Length (μm)	Taper Waist (μm)	Pump Power (mW)	Conversion Efficiency (dB)
BP	10^{-9} [31]	D-shaped fiber			~500	−71.1 [26]
BP	10^{-9} [31]	Microfiber	250	7	316	−59.15 [27]
Graphene	10^{-11} [23]	D-shaped fiber	150		100	−71.8 [28]
Antimonene	10^{-19} [24]	Microfiber	100	4.5	79	−63 [24]
GDY	10^{-9} [10]	Microfiber	860	5.6	6.93	−39.05 (this work)

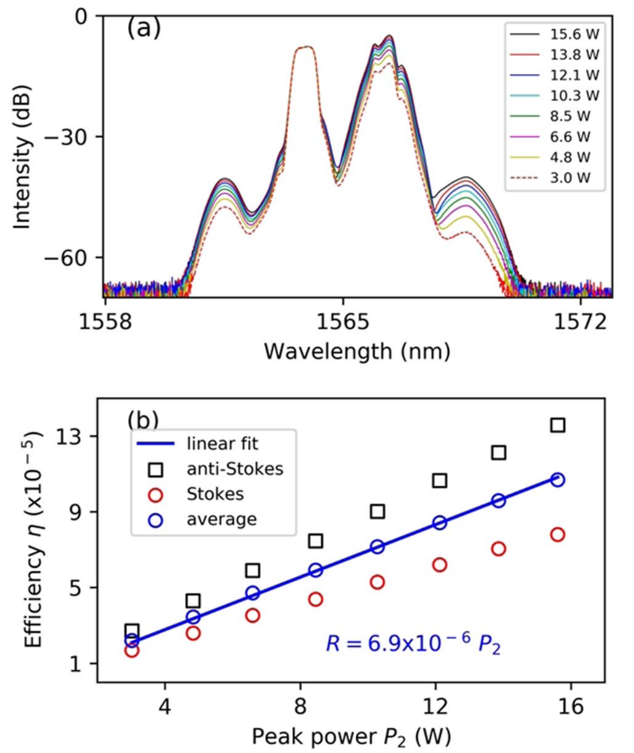

Fig. 6. FWM with the variation of the peak power of pump2. (a) FWM spectrum. (b) Conversion efficiency versus P_2.

incident average pump power, reducing possible damages to the 2D material-based devices.

This all-fiber FWM scheme can be a simple tool to estimate the γ of the nonlinear device. Compared with Z-scan that is usually employed to measure the nonlinear coefficient of the film type 2D material-based devices, the FWM scheme proposed here could be applied to microfiber type devices where nonlinear coefficients are not available by typical Z-scan measurement. As we set delay $= 0$ ps in our experiment, P_1 and P_2 represent the peak powers of the pump1 and pump2, respectively. By tuning the variable attenuator, the FWM spectra versus different P_2 are recorded [Fig. 6(a)]. We take both the anti-Stokes and Stokes signals into account and average the conversion efficiency to cancel the coupling power uncertainty. The conversion efficiency of the anti-Stokes and Stokes signals increases linearly with the increases of P_2, and the averaged result could be well fitted by the linear function with a slope of 6.9×10^{-6} [Fig. 6(b)]. As the slope $k = P_1(\gamma L)^2 \exp(-\alpha L)$, by substituting $P_1 = 7.37$ W, $\alpha = 431.5\ \mathrm{m}^{-1}$, and $L = 860$ μm into the formula, we estimate the γ of the GDY in our experiment to be 1354 W^{-1}/km.

Although the result of −39.05 dB in the manuscript has been improved by 20 dB compared to previous work by employing the all-fiber synchronized dual-wavelength pump source, there still needs more research to further improve the FWM efficiency. In the future, we will optimize the integration strategy and device parameters such as the absorption, deposition length, and taper waist to improve the nonlinearity of the device.

6. CONCLUSION

In summary, we have proposed an FWM scheme based on synchronized dual-wavelength pump pulses. The GDY-microfiber integrated in our scheme achieves a maximum conversion efficiency of −34.36 dB under the low average pump power of 6.93 mW. As the GDY contributes 34% to the whole FWM signal, the conversion efficiency of the GDY is −39.05 dB, which is improved by at least 20 dB compared to previously reported results. In addition, our proposed compact design provides an effective approach to measure the nonlinear coefficient of nanomaterials-based devices.

Funding. National Natural Science Foundation of China (51778030, 51978024, 8196130108).

Disclosures. The authors declare no conflicts of interest.

Data Availability. Data underlying the results presented in this paper are not publicly available at this time but may be obtained from the authors upon reasonable request.

†These authors contributed equally to this work.

REFERENCES

1. G. X. Li, Y. L. Li, H. B. Liu, Y. B. Guo, Y. J. Li, and D. B. Zhu, "Architecture of graphdiyne nanoscale films," Chem. Commun. **46**, 3256–3258 (2010).
2. Z. C. Zuo, H. Shang, Y. H. Chen, J. F. Li, H. B. Liu, Y. J. Li, and Y. L. Li, "A facile approach for graphdiyne preparation under atmosphere for an advanced battery anode," Chem. Commun. **53**, 8074–8077 (2017).
3. J. M. Liu, C. Y. Chen, and Y. L. Zhao, "Progress and prospects of graphdiyne-based materials in biomedical applications," Adv. Mater. **31**, 1804386 (2019).
4. J. Q. Li, J. Xu, Z. Q. Xie, X. Gao, J. Y. Zhou, Y. Xiong, C. G. Chen, J. Zhang, and Z. F. Liu, "Diatomite-templated synthesis of freestanding 3D graphdiyne for energy storage and catalysis application," Adv. Mater. **30**, 1800548 (2018).
5. Z. W. Jin, Q. Zhou, Y. H. Chen, P. Mao, H. Li, H. B. Liu, J. Z. Wang, and Y. L. Li, "Graphdiyne:ZnO nanocomposites for high-performance UV photodetectors," Adv. Mater. **28**, 3697–3702 (2016).

6. Y. Zhang, P. Huang, J. Guo, R. C. Shi, W. C. Huang, Z. Shi, L. M. Wu, F. Zhang, L. F. Gao, C. Li, X. W. Zhang, J. L. Xu, and H. Zhang, "Graphdiyne-based flexible photodetectors with high responsivity and detectivity," Adv. Mater. **32**, 2001082 (2020).
7. M. Q. Long, L. Tang, D. Wang, Y. L. Li, and Z. G. Shuai, "Electronic structure and carrier mobility in graphdiyne sheet and nanoribbons: theoretical predictions," ACS Nano **5**, 2593–2600 (2011).
8. G. van Miert, V. Juricic, and C. M. Smith, "Tight-binding theory of spin-orbit coupling in graphynes," Phys. Rev. B **90**, 195414 (2014).
9. Y. J. Li, L. Xu, H. B. Liu, and Y. L. Li, "Graphdiyne and graphyne: from theoretical predictions to practical construction," Chem. Soc. Rev. **43**, 2572–2586 (2014).
10. L. M. Wu, Y. Z. Dong, J. L. Zhao, D. T. Ma, W. C. Huang, Y. Zhang, Y. Z. Wang, X. T. Jiang, Y. J. Xiang, J. Q. Li, Y. Q. Feng, J. L. Xu, and H. Zhang, "Kerr nonlinearity in 2D graphdiyne for passive photonic diodes," Adv. Mater. **31**, 1807981 (2019).
11. J. Guo, R. C. Shi, R. Wang, Y. Z. Wang, F. Zhang, C. Wang, H. L. Chen, C. Y. Ma, Z. H. Wang, Y. Q. Ge, Y. F. Song, Z. Q. Luo, D. Y. Fan, X. T. Jiang, J. L. Xu, and H. Zhang, "Graphdiyne-polymer nanocomposite as a broadband and robust saturable absorber for ultrafast photonics," Laser Photon. Rev. **14**, 1900367 (2020).
12. J. Guo, Z. H. Wang, R. C. Shi, Y. Zhang, Z. W. He, L. F. Gao, R. Wang, Y. Q. Shu, C. Y. Ma, Y. Q. Ge, Y. F. Song, D. Y. Fan, J. L. Xu, and H. Zhang, "Graphdiyne as a promising mid-infrared nonlinear optical material for ultrafast photonics," Adv. Opt. Mater. **8**, 2000067 (2020).
13. R. I. Woodward and E. J. R. Kelleher, "2D saturable absorbers for fibre lasers," Appl. Sci. **5**, 1440–1456 (2015).
14. M. Zhang, Q. Wu, F. Zhang, L. Chen, X. Jin, Y. Hu, Z. Zheng, and H. Zhang, "2D black phosphorus saturable absorbers for ultrafast photonics," Adv. Opt. Mater. **7**, 1800224 (2019).
15. Q. Q. Hao, J. Guo, L. Y. Yin, T. Y. Ning, Y. Q. Ge, and J. Liu, "Watt-level ultrafast bulk laser with a graphdiyne saturable absorber mirror," Opt. Lett. **45**, 5554–5557 (2020).
16. J. Feng, X. Li, Z. Shi, C. Zheng, X. Li, D. Leng, Y. Wang, J. Liu, and L. Zhu, "2D ductile transition metal chalcogenides (TMCs): novel high-performance Ag_2S nanosheets for ultrafast photonics," Adv. Opt. Mater. **8**, 1901762 (2020).
17. J. Feng, X. Li, G. Zhu, and Q. J. Wang, "Emerging high-performance SnS/CdS nanoflower heterojunction for ultrafast photonics," ACS Appl. Mater. Interfaces **12**, 43098–43105 (2020).
18. X. Li, J. Feng, W. Mao, F. Yin, and J. Jiang, "Emerging uniform Cu_2O nanocubes for 251st harmonic ultrashort pulse generation," J. Mater. Chem. C **8**, 14386–14392 (2020).
19. J.-S. Liu, X.-H. Li, Y.-X. Guo, A. Qyyum, Z.-J. Shi, T.-C. Feng, Y. Zhang, C.-X. Jiang, and X.-F. Liu, "$SnSe_2$ nanosheets for subpicosecond harmonic mode-locked pulse generation," Small **15**, 1902811 (2019).
20. Y. Zhao, W. Wang, X. Li, H. Lu, Z. Shi, Y. Wang, C. Zhang, J. Hu, and G. Shan, "Functional porous MOF-derived CuO octahedra for harmonic soliton molecule pulses generation," ACS Photon. **7**, 2440–2447 (2020).
21. Y. Zhao, P. Guo, X. Li, and Z. Jin, "Ultrafast photonics application of graphdiyne in the optical communication region," Carbon **149**, 336–341 (2019).
22. G. Agrawal, "Chapter 10—four-wave mixing," in *Nonlinear Fiber Optics*, 5th ed., G. Agrawal, ed. (Academic, 2013), pp. 397–456.
23. H. Zhang, S. Virally, Q. L. Bao, L. K. Ping, S. Massar, N. Godbout, and P. Kockaert, "Z-scan measurement of the nonlinear refractive index of graphene," Opt. Lett. **37**, 1856–1858 (2012).
24. Y. F. Song, Y. X. Chen, X. T. Jiang, W. Y. Liang, K. Wang, Z. M. Liang, Y. Q. Ge, F. Zhang, L. M. Wu, J. L. Zheng, J. H. Ji, and H. Zhang, "Nonlinear few-layer antimonene-based all-optical signal processing: ultrafast optical switching and high-speed wavelength conversion," Adv. Opt. Mater. **6**, 1701287 (2018).
25. Y. Wu, Q. Wu, F. Sun, C. Cheng, S. Meng, and J. Zhao, "Emergence of electron coherence and two-color all-optical switching in MoS_2 based on spatial self-phase modulation," Proc. Natl. Acad. Sci. USA **112**, 11800–11805 (2015).
26. S. Uddin, P. C. Debnath, K. Park, and Y. W. Song, "Nonlinear black phosphorus for ultrafast optical switching," Sci. Rep. **7**, 43371 (2017).
27. J. L. Zheng, Z. H. Yang, C. Si, Z. M. Liang, X. Chen, R. Cao, Z. N. Guo, K. Wang, Y. Zhang, J. H. Ji, M. Zhang, D. Y. Fan, and H. Zhang, "Black phosphorus based all-optical-signal-processing: toward high performances and enhanced stability," ACS Photon. **4**, 1466–1476 (2017).
28. P. C. Debnath, S. Uddin, and Y. W. Song, "Ultrafast all-optical switching incorporating in situ graphene grown along an optical fiber by the evanescent field of a laser," ACS Photon. **5**, 445–455 (2018).
29. Y. Wu, B. C. Yao, Y. Cheng, Y. J. Rao, Y. Gong, X. Y. Zhou, B. J. Wu, and K. S. Chiang, "Four-wave mixing in a microfiber attached onto a graphene film," IEEE Photon. Technol. Lett. **26**, 249–252 (2014).
30. M. M. Haley, S. C. Brand, and J. J. Pak, "Carbon networks based on dehydrobenzoannulenes: synthesis of graphdiyne substructures," Angew. Chem. Int. Ed. **36**, 836–838 (1997).
31. J. D. Zhang, X. F. Yu, W. J. Han, B. S. Lv, X. H. Li, S. Xiao, Y. L. Gao, and J. He, "Broadband spatial self-phase modulation of black phosphorous," Opt. Lett. **41**, 1704–1707 (2016).
32. X. X. Jin, G. H. Hu, M. Zhang, T. Albrow-Owen, Z. Zheng, and T. Hasan, "Environmentally stable black phosphorus saturable absorber for ultrafast laser," Nanophotonics **9**, 2445–2449 (2020).
33. X. X. Jin, G. H. Hu, M. Zhang, Y. W. Hu, T. Albrow-Owen, R. C. T. Howe, T. C. Wu, Q. Wu, Z. Zheng, and T. Hasan, "102 fs pulse generation from a long-term stable, inkjet-printed black phosphorus-mode-locked fiber laser," Opt. Express **26**, 12506–12513 (2018).
34. G. H. Hu, L. S. Yang, Z. Y. Yang, Y. B. Wang, X. X. Jin, J. Dai, Q. Wu, S. H. Liu, X. X. Zhu, X. S. Wang, T. C. Wu, R. C. T. Howe, T. Albrow-Owen, L. W. T. Ng, Q. Yang, L. G. Occhipinti, R. I. Woodward, E. J. R. Kelleher, Z. P. Sun, X. Huang, M. Zhang, C. D. Bain, and T. Hasan, "A general ink formulation of 2D crystals for wafer-scale inkjet printing," Sci. Adv. **6**, eaba5029 (2020).
35. D. K. Sang, H. Wang, Z. Guo, N. Xie, and H. Zhang, "Recent developments in stability and passivation techniques of phosphorene toward next-generation device applications," Adv. Funct. Mater. **29**, 1903419 (2019).
36. K. K. Chow and S. Yamashita, "Four-wave mixing in a single-walled carbon-nanotube-deposited D-shaped fiber and its application in tunable wavelength conversion," Opt. Express **17**, 15608–15613 (2009).
37. M. Zhang, E. J. R. Kelleher, A. S. Pozharov, E. D. Obraztsova, S. V. Popov, and J. R. Taylor, "Passive synchronization of all-fiber lasers through a common saturable absorber," Opt. Lett. **36**, 3984–3986 (2011).
38. J. Sotor, G. Sobon, J. Tarka, I. Pasternak, A. Krajewska, W. Strupinski, and K. M. Abramski, "Passive synchronization of erbium and thulium doped fiber mode-locked lasers enhanced by common graphene saturable absorber," Opt. Express **22**, 5536–5543 (2014).
39. D. Yoshitomi and K. Torizuka, "Long-term stable passive synchronization between two-color mode-locked lasers with the aid of temperature stabilization," Opt. Express **22**, 4091–4097 (2014).
40. N. Shibata, R. Braun, and R. Waarts, "Phase-mismatch dependence of efficiency of wave generation through four-wave mixing in a single-mode optical fiber," IEEE J. Quantum Electron. **23**, 1205–1210 (1987).
41. K. K. Chow, M. Tsuji, and S. Yamashita, "Single-walled carbon-nanotube-deposited tapered fiber for four-wave mixing based wavelength conversion," Appl. Phys. Lett. **96**, 061104 (2010).